

Resolved Versus Parametrized Boundary-Layer Plumes. Part II: Continuous Formulations of Mixing Rates for Mass-Flux Schemes

C. Rio · F. Hourdin · F. Couvreux · A. Jam

Received: 24 February 2009 / Accepted: 16 February 2010 / Published online: 5 March 2010
© Springer Science+Business Media B.V. 2010

Abstract The conditional sampling of coherent structures in large-eddy simulations of the convective boundary layer (Couvreux et al. Boundary-layer Meteorol 134:441–458, 2010) is used to propose and evaluate formulations of fractional entrainment and detrainment rates for mass-flux schemes. The proposed formulations are physically-based and continuous from the surface to the top of clouds. Entrainment is related to the updraft vertical velocity divergence, while detrainment depends on the thermal vertical velocity, on buoyancy and on the moisture contrast between the mean plume and its environment. The proposed formulations are first directly evaluated in simulations of shallow clouds. They are then tested in single-column simulations with the thermal plume model, a mass-flux representation of boundary-layer thermals.

Keywords Boundary-layer thermals · Entrainment and detrainment · Large-eddy simulations · Mass-flux parametrization

1 Introduction

Boundary-layer turbulence and shallow clouds are classically handled separately in large-scale models. The diffusive approach is used to represent the local transport within the boundary layer, while the effects of cumulus clouds are often parametrized using a mass-flux approach initialized at cloud base. However, observations show that the major part of the vertical transport is carried out by coherent structures within the convective boundary layer and that cumulus clouds are the saturated part of thermals originating from the surface layer (LeMone and Pennell 1976). To represent the non-local transport in large-scale models, several methods have been explored, such as the introduction of a counter-gradient

C. Rio (✉) · F. Couvreux
GAME Meteo-France and CNRS, 42 Coriolis, 31057 Toulouse, France
e-mail: catherine.rio@lmd.jussieu.fr

F. Hourdin · A. Jam
LMD-IPSL, pl Jussieu, 75005 Paris, France

term (Deardorff 1972), transilient matrices (Stull 1984), or the mass-flux approach (Chatfield and Brost 1987; Siebesma and Teixeira 2000; Houdin et al. 2002). The advantage of the last approach is that the mass-flux scheme for the sub-cloud layer can be extended to the cloud layer, thus representing boundary-layer thermals and cumulus clouds in a unified way (among others Soares et al. 2004; Rio and Houdin 2008; Pergaud et al. 2009). In this approach, each grid cell is decomposed into an updraft, of mass flux f and vertical velocity w_u covering a fraction α , with $f = \alpha\rho w_u$ (ρ being the air density), and its environment. The vertical variation of f relies on the entrainment of air inside the plume e and detrainment of air from the plume d , where

$$\frac{\partial f}{\partial z} = e - d. \quad (1)$$

So-called fractional entrainment and detrainment rates are defined by $\varepsilon = e/f$ and $\delta = d/f$.

Internal variables of the scheme, i.e. the mean thermal characteristics such as the thermal vertical velocity, fractional cover, mass flux and mixing rates, are difficult to retrieve from observations. The evaluation of their representation in mass-flux parametrizations thus generally relies on large-eddy simulations (LES), whose resolution is fine enough to explicitly account for coherent structures within the dry (Moeng and Wyngaard 1988; Couvreux et al. 2005) and cloudy (Brown et al. 2002; Siebesma et al. 2003) convective boundary layers. LES also reproduce satisfactorily the statistical properties of clouds (Siebesma and Jonker 2000; Neggers et al. 2003). A key issue for model evaluation is the method used to sample coherent structures in LES.

The first part of our study (Couvreux et al. 2010) proposes a new conditional sampling of boundary-layer plumes that allows the characterization of thermals continuously from the surface to the top of the dry or cloudy boundary layer in LES. This sampling is based on the combination of thermodynamic variables and a tracer emitted at the surface with a lifetime of typically 15 min. It allows the filling of the gap between criteria used to select dry thermals in the lower part of the boundary layer [seen as ascending (Young 1988), positively buoyant (Williams and Hacker 1992) or ascending moist (Grossman 1984) plumes] and those used to select clouds [characterized as liquid parcels, possibly ascending and buoyant (Siebesma and Cuijpers 1995)]. In particular, the approach is valid at the top of the sub-cloud layer, in the detrainment zone of dry thermals. In part II, we show how this sampling can be used to evaluate a mass-flux representation of thermals and in particular to evaluate physically-based continuous formulations for fractional entrainment and detrainment rates between the mean plume and its environment.

Observations of clouds have led to several controversies about dominant mixing processes between a cloud and its environment. Some studies emphasize the fact that cloudy parcels are a combination of air from cloud base and air from levels higher than cloud top (Paluch 1979) and the importance of cloud-top entrainment (Blyth et al. 1988), while others highlight lateral mixing at all cloud levels (Stith 1992; Heus et al. 2008). Besides the progress in the understanding of mixing processes in individual clouds, thanks to recent tracer studies (Zhao and Austin 2005; Heus et al. 2008), the specification of fractional mixing rates used in mass-flux schemes is still an open issue. Two types of approaches are used to represent mixing in shallow clouds: episodic mixing and buoyancy sorting (Bretherton et al. 2004) or entraining/detraining plume (Soares et al. 2004; Rio and Houdin 2008) models. For the latter approach, Siebesma and Cuijpers (1995) show, using LES, that fractional mixing rates can be defined, as a first approximation, as constant inside clouds: ε is inversely proportional to a typical cloud radius, while δ is larger than ε , so that the mass-flux decreases from the base to the top of the cloud layer. Since then, several studies have tried to refine those definitions

by relating the fractional entrainment rate to plume characteristics (Neggers et al. 2002) or differences between clouds and environmental conditions (Von Salzen and McFarlane 2002; Gregory 2001). As for detrainment, de Rooy and Siebesma (2008) propose a formulation relating the fractional detrainment rate to the buoyancy excess of the plume and the relative humidity of environmental air. Mixing processes have been less studied in the sub-cloud layer, between dry thermals and their environment, probably because of the lack of a sampling criterion to characterize dry thermals in the upper part of the boundary layer. Here, we derive from physical considerations continuous formulations for the fractional entrainment and detrainment rates valid both in the dry and the cloudy parts of the mean thermal. The conditional sampling presented in part I is then used to evaluate those formulations and fix values for the free parameters. Finally, the formulations are implemented in the thermal plume model of Rio and Hourdin (2008) and tested in single-column simulations of the cloudy convective boundary layer.

Section 2 revisits the definition of the sampling introduced in part I. In Sect. 3, the conditional sampling is used to evaluate a formulation of fractional entrainment rate derived from physical considerations, and to highlight correlations between the fractional detrainment rate and contrasts between the mean plume and its environment. Section 4 presents results obtained when the formulations are implemented in the thermal plume model, a mass-flux scheme for boundary-layer thermals. Conclusions are drawn in Sect. 5.

2 A Conditional Sampling to Evaluate Mass-Flux Schemes

In the mass-flux scheme formalism retained for the conditional sampling and thermal plume model, any conserved variable ψ (liquid potential temperature θ_l or total water r_t) is transported inside the updraft and satisfies,

$$\frac{\partial f \psi_u}{\partial z} = e\psi - d\psi_u \quad (2)$$

assuming that the plume (subscript ‘u’) is in steady state and that environmental values are equal to large-scale values (ψ). Conservation equations depend on mixing rates e and d for which no prognostic nor diagnostic equations exist a priori and which need to be specified in the parametrization. Here, we use LES to evaluate formulations of the fractional mixing rates.

In order to separate thermal plumes from their environment, a new conditional sampling was proposed in Part I, which is based on the combination of thermodynamic variables and the concentration of a passive tracer emitted at the surface. The lifetime is fixed here to 15 min. As the tracer is transported within thermals before being detrained to the environment, thermals can be characterized by:

$$sv' > \max(\sigma_{sv}, \sigma_{min}) \quad \text{and} \quad w > 0,$$

where $sv'(w)$ is the scalar (vertical velocity) anomaly, σ_{sv} the standard deviation of the scalar at a given vertical level and σ_{min} is a minimum threshold. For shallow cumulus clouds, a condition on a positive liquid water content ($r_l > 0$) is added above the quarter of the cloud layer, to distinguish cloudy parcels from detrained air.

The proposed sampling is consistent with the representation of convective updrafts by mass-flux schemes, considered as ascending and buoyant plumes supplied with air coming from the surface layer (see Couvreux et al. 2010).

3 Using LES to Evaluate Continuous Formulations of Mixing Rates

From the equations of mass (Eq. 1) and the conservation of variable ψ (Eq. 2) we deduce:

$$\frac{\partial \psi_u}{\partial z} = \varepsilon(\psi - \psi_u), \quad (3)$$

where the fractional entrainment rate drives plume characteristics. The fractional detrainment rate ($\delta = d/f$) is deduced from Eq. 1, via

$$\delta = \frac{-1}{f} \frac{\partial f}{\partial z} + \varepsilon, \quad (4)$$

where detrainment affects the mass flux and thus the fractional cover of the plume.

3.1 Entrainment

Let us first consider an idealized situation with no entrainment nor detrainment. When the thermal plume accelerates, the horizontal section of the mean thermal plume (or fractional cover of the ensemble of plumes) decreases in order to conserve the mass flux. At the other extreme, it could be assumed that lateral entrainment compensates exactly this narrowing, so as to keep the thermal section constant in the absence of detrainment. In this extreme view, proposed in previous studies (Nordeng 1994; Siebesma 1998), we have (neglecting the variation of ρ):

$$\varepsilon = \frac{1}{f} \frac{\partial f}{\partial z} = \frac{1}{w_u} \frac{\partial w_u}{\partial z}. \quad (5)$$

Here, we argue that the effective entrainment rate lies between these two extreme views, so that we have:

$$\varepsilon = \max \left(0, \frac{\beta_1}{w_u} \frac{\partial w_u}{\partial z} \right), \quad (6)$$

with $0 \leq \beta_1 \leq 1$.

In order to test this hypothesis, we apply the conditional sampling to two simulations of shallow convection, one over the land (ARM, Brown et al. 2002) and one over the ocean (BOMEX, Siebesma et al. 2003), the set-up of which are described in more details in Couvreux et al. (2010). On the one hand the vertical divergence of w_u can be diagnosed from LES using the average of w_u over the sampled region, while on the other hand entrainment can be computed from (Siebesma and Cuijpers 1995):

$$\varepsilon = \frac{1}{\psi - \psi_u} \frac{\partial \psi_u}{\partial z}, \quad (7)$$

where ψ is a conserved variable (either θ_l , r_t or s_v). Note that Eq. 7 is not an exact formulation of the fractional entrainment rate. It assumes stationary conditions and neglects the intra-structure turbulence, which can lead to an overestimation of the fractional entrainment rate of 30% near cloud base and top (Siebesma and Cuijpers 1995). However, the same assumptions are made in mass-flux schemes.

Figure 1 shows the vertical profiles of ε for two hours of the ARM simulation (ARM7 and ARM9, corresponding to 1330 local time and 1530 local time respectively) and the fifth hour of the BOMEX simulation (BOM5), as obtained from LES using the cloud (red triangles), the core (green squares) and the new (black dots) samplings. Note that the new sampling leads to fractional entrainment rates lying between the classical cloud and core estimates in the cloud

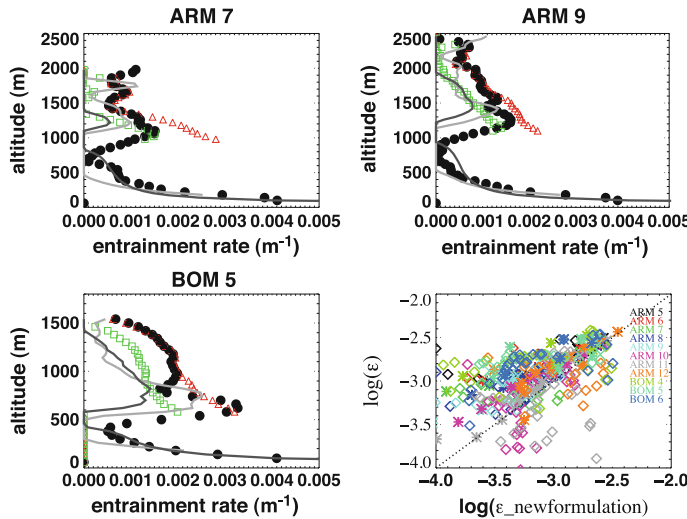


Fig. 1 Fractional entrainment rate ε . Comparison of vertical profiles of ε obtained from the cloud (red triangles), core (green squares) and new (black dots) samplings with the proposed formulation (Eq. 6, $\beta_1 = 0.9$, light grey) and $\frac{a_1 \beta_1}{1+\beta_1} \frac{B}{w_u^2}$ (with $a_1 = 2/3$, dark grey). Results are displayed at 1330 local time (ARM7, *upper left*) and 1530 local time (ARM9, *upper right*) for simulation ARM and at the fifth hour of simulation BOMEX (BOM5, *lower left*). The *lower right panel* displays (logarithmic scale) the fractional entrainment rate as a function of the new formulation for all levels and all hours of simulations ARM and BOMEX, in both the sub-cloud (*stars*) and the cloud (*diamonds*) layers

layer. The light grey line corresponds to Eq. 6 for $\beta_1 = 0.9$. Vertical variations of the vertical velocity divergence indeed follow that of ε for the three hours considered here, both in the sub-cloud and the cloud layers. The entrainment rate decreases from the surface to a location right beneath cloud base, where it increases rapidly and then decreases from cloud base to cloud top, with a possible second increase near cloud top. Major discrepancies between ε and the proposed formulation are seen near cloud base. This figure also highlights the limitations of taking constant values for ε inside clouds, as is done in many parametrizations using entraining plumes (Tiedtke 1989; Soares et al. 2004; Rio and Houdin 2008).

The fractional entrainment rate is plotted as a function of the formulation given by Eq. 6 with $\beta_1 = 0.9$ for all levels and hours of ARM and BOMEX simulations (Fig. 1, lower right panel). Two different marks are used to distinguish the cloud (diamonds) from the sub-cloud layer (stars). Results show a reasonable correlation between entrainment and the divergence of the vertical velocity, both in the cloud and sub-cloud layers. This suggests that β_1 is close to one, as in the constant fraction hypothesis.

3.2 The Vertical Velocity Equation

For the vertical momentum w_u , assuming that the air is entrained inside the plume with a zero vertical velocity, the conservation Eq. 2 for the thermal plume can be expressed formally as

$$\frac{\partial f w_u}{\partial z} = -dw_u + \alpha\rho\Gamma, \quad (8)$$

where Γ is an equivalent specific force applied to the plume air parcels. Combining the equations of conservation of mass Eq. 1 and momentum (Eq. 8) leads to:

$$\frac{1}{2} \frac{\partial w_u^2}{\partial z} = -w_u^2 \varepsilon + \Gamma. \quad (9)$$

Here Γ accounts for the effective external forces, such as thermal buoyancy, vertical momentum fluxes associated with sub-thermal fluctuations, and vertical pressure torques on the plume boundaries. According to [Gregory \(2001\)](#),

$$\Gamma = B - \frac{1}{\alpha \rho} \frac{\partial \alpha \rho \overline{w_u'^2}}{\partial z} - \frac{1}{\rho} \frac{\partial \overline{p'}}{\partial z} - g \frac{\overline{p'}}{p}, \quad (10)$$

where $B = g(\overline{\theta_{vu}} - \overline{\theta_v})/\theta_v$ is the plume buoyancy, p is the pressure and the prime denotes a perturbation around a mean state, and the overbar is the mean over the thermal.

The parametrization of pressure and turbulence terms in Eq. 10 is still an issue for mass-flux schemes. Classically, the turbulence term is taken as proportional to the buoyancy term, while pressure perturbations are taken proportional to the entrainment term, leading to ([Simpson and Wiggert 1969; Siebesma et al. 2003](#)):

$$\frac{1}{2} \frac{\partial w_u^2}{\partial z} = a_1 B - a_2 \varepsilon w_u^2, \quad (11)$$

where coefficients a_1 ranges from 1/6 to 2/3 and a_2 from 1 to 2. However, such relations still need to be demonstrated. [Gregory \(2001\)](#) remarks that taking the pressure perturbation term proportional to entrainment leads to drag that is too small inside clouds when entrainment is not taken constant but decreasing with height. He rather proposes to take this term proportional to detrainment, which increases with height. This issue is not addressed here. For simplicity, we take into account the impact of turbulence growth by reducing the buoyancy term, and the effect of pressure perturbations by adding a constant drag term, so that:

$$\Gamma = a_1 B - b w_u^2 \quad (12)$$

where a_1 and b are free parameters. Those parameters are fixed by comparing the profiles of vertical velocity from LES to the one simulated with the thermal plume model (see Sect. 4), leading to $a_1 = 2/3$ and $b = 0.002$, values consistent with previous studies.

Note that combining Eq. 9, Eq. 6 and Eq. 12 leads to the following definition of ε in the parametrization world:

$$\varepsilon = \max \left(0, \frac{1}{1 + \beta_1} \left(a_1 \frac{B}{w_u^2} - b \right) \right). \quad (13)$$

[Gregory \(2001\)](#) also proposed a relationship between ε and B/w_u^2 :

$$\varepsilon = A \frac{B}{w_u^2} \quad (14)$$

where $A \approx 0.08$ (Here, we have $a_1 \beta_1 (1 + \beta_1)^{-1} = 0.315$). In the [Gregory \(2001\)](#) formulation, drag does not affect entrainment while here we argue that it does. Vertical variations of the ratio of buoyancy versus the square of vertical velocity are thus also plotted in Fig. 1 (dark grey). This ratio also shows good consistency with the fractional entrainment rate, but underestimates it near cloud base and top. The vertical velocity divergence appears to be a somewhat better approximation of ε than the ratio of buoyancy versus the square of the vertical velocity.

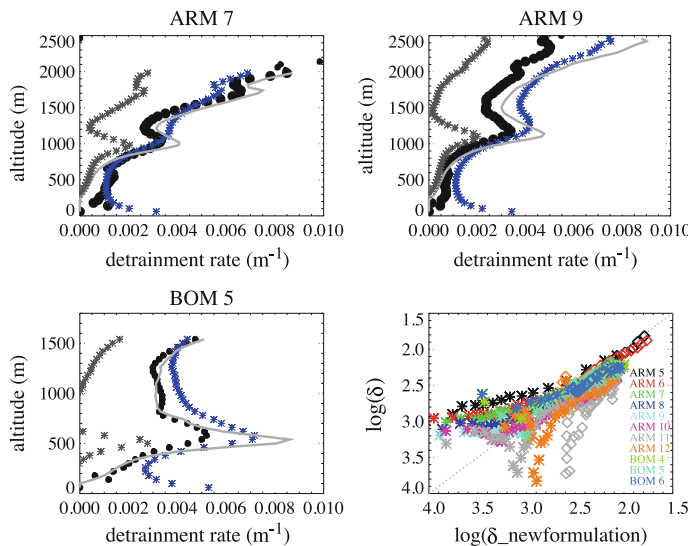


Fig. 2 Fractional detrainment rate δ . Comparison of vertical profiles of δ obtained from the new sampling (black dots) with $-\frac{a_1\beta_1}{1+\beta_1}\frac{B}{w_u^2} + 0.001$ ($a_1 = 2/3$, $\beta_1 = 0.9$ and 0.001 is added to visualize the profiles on the graph, grey stars), and the proposed formulation (Eq. 15, light grey line). Results are displayed at 1330 local time (ARM7, upper left) and 1530 local time (ARM9, upper right) for simulation ARM and at the fifth hour of simulation BOMEX (BOM5, lower left). The lower right panel displays (logarithmic scale) the fractional detrainment rate as a function of the new formulation for all levels and all hours of simulations ARM and BOMEX, in both the sub-cloud (stars) and the cloud (diamonds) layers

3.3 Detrainment

With the same arguments as for entrainment, it could be expected that a deceleration of the plume will be associated with detrainment, in particular in overshooting regions where the buoyancy is strongly negative. Observations also suggest that detrainment is favoured in regions where buoyancy is negative or decreasing with height (Bretherton and Smolarkiewicz 1989). The divergence of air due to negative buoyancy might favour the detrainment of air from the plume, while the convergence of air due to positive buoyancy might act against it. The buoyancy contribution to the vertical velocity divergence is $a_1\beta_1 B/(w_u^2(1+\beta_1))$. We might also expect a correlation between the fractional detrainment rate δ and B/w_u^2 .

Another interpretation for this effect of buoyancy is that air parcels extracted by turbulence at the edges of the plume may fall down when their buoyancy is negative while they may continue to rise if it is positive (and may thus in particular still be considered as plume parcels when applying the conditional sampling). This kind of consideration is at the basis of the buoyancy sorting approach. Evaporation of parcels at the edges of clouds (Nordeng 1994; Siebesma 1998) can also play a role then, by reinforcing the negative buoyancy of the extracted air parcel. Recent LES experiments have shown that the evaporative cooling at the edges of clouds induces subsiding shells (Heus and Jonker 2008), shown to affect the trajectory of detrained parcels (Heus et al. 2008). We might thus expect that detrainment also occurs at the small scale, via the subsiding shells driven by the evaporation at the edges of clouds. This mechanism is enhanced when the moisture contrast between the clouds and

the environment increases, and this contrast might also affect detrainment in the dry part of thermals. These considerations led us to explore relationships between δ and plume and environmental characteristics, such as $\delta = F(B, w_u, \Delta r_t/r_t)$, where $\Delta r_t = r_{tu} - r_t$.

In Fig. 2, the vertical profile of δ diagnosed from LES using the new sampling is shown as black dots for ARM7, ARM9 and BOM5. The grey stars correspond to the vertical profile of $-a_1\beta_1 B/w_u^2(1 + \beta_1)$ (with $\beta_1 = 0.9$ and $a_1 = 2/3$, using the same scaling as for entrainment) and the purple stars to the vertical profile of $c((\Delta r_t/r_t)/w_u^2)^d$ (with $c = 0.012$ and $d = 0.5$). These plots clearly illustrate that δ is rather well correlated with both $-B/w_u^2$ and $(\Delta r_t/r_t)/w_u^2$. Detrainment is enhanced in regions of negative buoyancy, where the vertical velocity decreases, near cloud base and top, but also constantly increases with height as does the moisture contrast between the plume and its environment. Here the LES results help us visualise these correlations, but cannot be used to determine independently the values of the free parameters. After a series of tests using both LES and results from the thermal plume model (see Sect. 4), we propose the following definition:

$$\delta = \max \left(0, -\frac{a_1\beta_1}{1 + \beta_1} \frac{B}{w_u^2} + c \left(\frac{\Delta r_t/r_t}{w_u^2} \right)^d \right) \quad (15)$$

with $a_1 = 2/3$, $\beta_1 = 0.9$, $c = 0.012 \text{ s}^{-1}$ and $d = 0.5$. This formulation is shown as the light grey line on the vertical profiles in Fig. 2 and shows reasonable agreement with δ directly computed from conserved variables. On the fourth panel of the figure (lower right), the fractional detrainment rate is plotted as a function of the new formulation for all levels and hours of the ARM and BOMEX simulations (stars represent the sub-cloud layer and diamonds represent the cloud layer). Main discrepancies seem to occur in the sub-cloud layer.

4 Application to the Thermal Plume Model

4.1 Introducing the Formulations in the Thermal Plume Model

The formulations are introduced in the thermal plume model of [Rio and Hourdin \(2008\)](#) (see also [Hourdin et al. 2002](#); [Coindreau et al. 2007](#)), a mass-flux scheme that aims to represent the vertical transport by coherent structures within the convective boundary layer. The specificity of the scheme is to represent the ensemble of thermals within a grid cell by a unique mean ascending thermal plume, which can be dry or cloudy. The plume is initialized in the surface layer (with $w_{u0} = 0$, $\theta_{lu0} = \theta_{l0}$, $r_{tu0} = r_{l0}$ at the surface), so that characteristics of the plume are continuous from the surface to the cloud top, with no triggering function at cloud base. The equations include the conservation of mass, momentum, liquid potential temperature and total water. Note that horizontal momentum is also transported by the scheme. The closure equation relates the mass flux at the top of the unstable surface layer to the horizontal convergence of air in the surface layer (see [Rio and Hourdin \(2008\)](#) for more details). The thermal plume model is combined with an eddy-diffusivity approach so that the vertical flux of a quantity ψ is expressed by:

$$\rho \overline{w' \psi'} = -\rho K_z \frac{\partial \psi}{\partial z} + f(\psi_u - \psi), \quad (16)$$

and where computation of K_z relies on a prognostic equation for the turbulent kinetic energy ([Yamada 1983](#)).

In the original version of the scheme (Rio and Hourdin 2008), the lateral detrainment rate d is deduced from geometrical considerations in the sub-cloud layer while δ is taken as a constant in the cloud layer ($\delta = 2 \times 10^{-3} \text{ m}^{-1}$). The lateral entrainment rate is defined as a constant fraction (0.4) of the detrainment rate all along the plume (so that $\varepsilon = 0.8 \times 10^{-3} \text{ m}^{-1}$ inside clouds). These values were tuned to fit the vertical profiles of large-scale variables for the ARM case, and are comparable with the Siebesma and Cuijpers (1995) estimates: $1.5\text{--}2.5 \times 10^{-3} \text{ m}^{-1}$ for ε and $2.5\text{--}3 \times 10^{-3} \text{ m}^{-1}$ for δ inside clouds.

The formulations of ε and δ presented in the previous section (Eqs. 13, 15), valid from the surface to cloud top, are introduced into the thermal plume model. The equation for the conservation of momentum is also modified according to Eqs. 9, 12, therefore including the effect of drag and small-scale turbulence not accounted for in the original version. The thermal plume model is operated in the single-column version of the LMDz general circulation model (Hourdin et al. 2006) on the ARM and BOMEX cases following Brown et al. (2002) and Siebesma et al. (2003) for the simulation set-ups. Results are shown for simulations using 40 layers in the first 4 km for the ARM case and 75 layers for the BOMEX case, and a time step of 20 s.

4.2 Representation of Internal Variables of the Scheme

Fractional mixing rates ε and δ obtained with the original (TH) and the new (THnew) versions of the scheme are compared with LES in Fig. 3 at 1330 local time (ARM7) and 1530 local time (ARM9) for the ARM case and at the fifth hour of the BOMEX simulation (BOM5). The new conditional sampling first offers an opportunity to evaluate the representation of entrainment and detrainment rates in the original version of the scheme. As already mentioned, the tuning of free parameters in that version was done by fitting the large-scale vertical profiles only. The values of the entrainment and detrainment rates obtained are however in reasonable agreement with LES for the ARM case, in particular for the entrainment rate in the sub-cloud layer. The rates are strongly underestimated inside clouds for the BOMEX case. The comparison also underlines the limitation of taking constant values for ε and δ in the cloud layer, as those rates appear to vary in space and time.

Concerning the new version of the model, the agreement between the new formulations of ε and δ and LES results is similar to that shown in Figs. 1, 2. Differences arise from the fact that LES values of ε and δ are here compared with those obtained using the internal variables given by the thermal plume model in the framework of single-column simulations over several hours. In Figs. 1, 2, the variables used in the formulations were issued from the same LES simulation using the conditional sampling. It is thus the full model that is tested here, and not only the relationship between ε or δ and the internal variables. The overall agreement is satisfying, and even somewhat better than in Fig. 1 for the entrainment within clouds for the ARM case, while the formulation somewhat underestimates entrainment inside clouds for the BOMEX case in both LES and single-column simulations, a quite robust feature that may deserve further investigation.

Figure 4 displays the comparison for TH and THnew with large-eddy simulations of other internal variables of the scheme: the fractional cover α , the vertical velocity w_u and the mass flux f . Despite approximate formulations of mixing rates in TH, the vertical mass flux is quite consistent with LES. This suggests that a correct representation of $\varepsilon - \delta$ is more important than a correct representation of these rates independently in order to have a good representation of the mass flux on a given case study. On the other hand, the vertical velocity was really overestimated in the initial version of the scheme, in which drag and pressure perturbations were neglected, and which led to a strong underestimation of the fractional

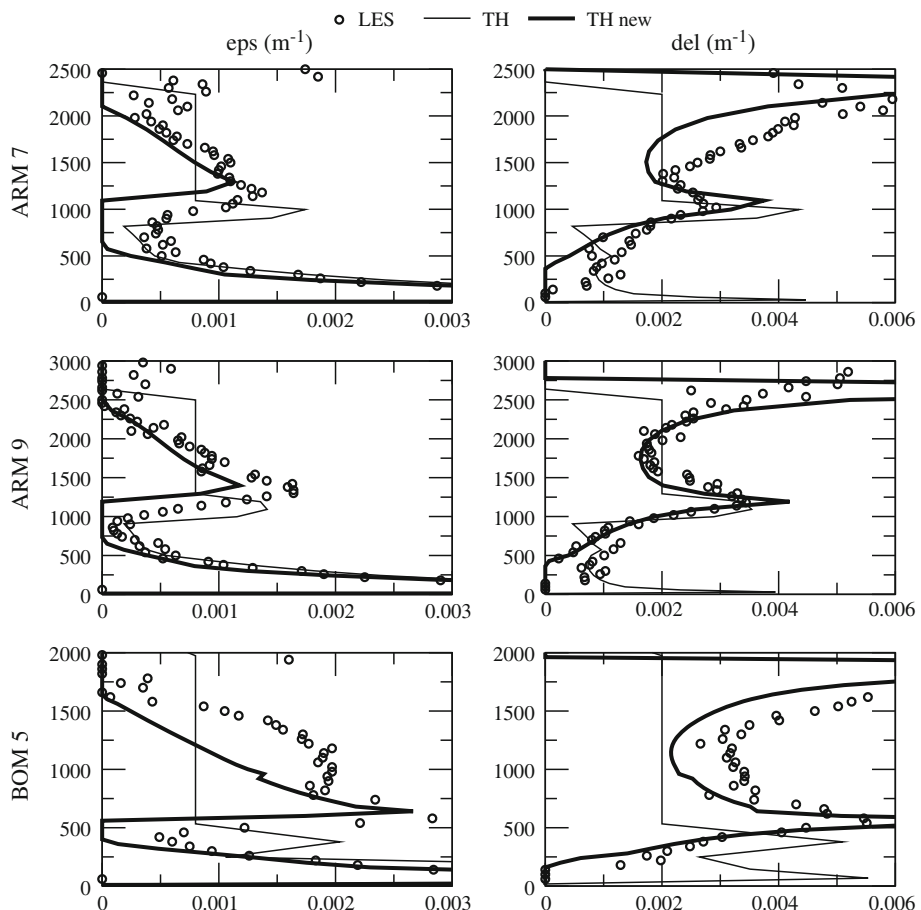


Fig. 3 Vertical profiles of fractional entrainment (ε in m^{-1} , left) and detrainment (δ in m^{-1} , right) rates at 1330 local time (ARM7) and 1530 local time (ARM9) for the ARM case and at the fifth hour of simulation BOMEX (BOM5): comparison of LES results using the conditional sampling (black dots) with results obtained with the original (TH, light black line) and the new (THnew, dark black line) versions of the thermal plume model

cover of the plume. Both the vertical velocity equation and the definition of mixing rates are important for reproducing realistic plume properties. The new scheme, with its better representation of mixing rates and effect of drag and turbulence, allows an improvement of the vertical profile of the vertical velocity, while maintaining a mass flux consistent with LES, leading to a better representation of the plume coverage. This fraction is somewhat overestimated in the sub-cloud layer, due to an overestimation of the mass flux, probably related to an underestimation of δ in the sub-cloud layer.

4.3 Representation of Vertical Fluxes and Mean Profiles

The corresponding parametrized fluxes and variances are compared with the top-hat contribution to the total fluxes and variances¹ simulated by LES in Fig. 5 for θ_l . The representation of the vertical flux is improved (left), as is the variance (right), due in particular to a better

¹ Note that the top-hat contribution underestimates total fluxes and variances, see part I.

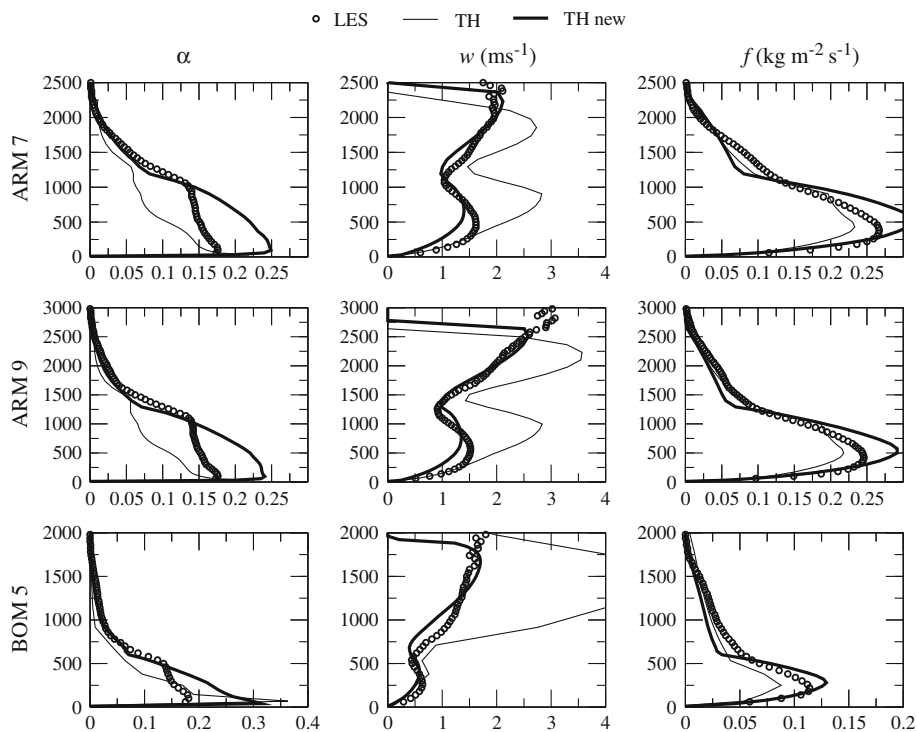


Fig. 4 Vertical profiles of the thermal fractional cover (α , left), vertical velocity (w in m s^{-1} , middle) and mass flux (f in $\text{kg m}^{-2} \text{s}^{-1}$, right) at 1330 local time (ARM7) and 1530 local time (ARM9) for the ARM case and at the fifth hour of simulation BOMEX (BOM5): comparison of LES results using the conditional sampling (black dots) with results obtained with the original (TH, light black line) and the new (THnew, dark black line) versions of the thermal plume model

representation of the fractional cover. Thus, the better representation of the internal variables of the scheme, based on improved physical concepts, helps improvement of the representation of vertical fluxes and variances, both for the ARM and BOMEX simulations. Vertical profiles of liquid potential temperature and total water are still well reproduced, as illustrated in Fig. 6. However, there are still discrepancies with the LES results, particularly near cloud base for the ARM case, where the environment is too dry and too warm. In fact, sensitivity tests show that, at this stage, tuning more accurately internal variables of the scheme and thus top-hat contribution to vertical fluxes, can worsen the mean profiles obtained. This may be related to the fact that, in the single-column simulations, the whole vertical transport is carried out by thermals (except in the surface layer where diffusion contributes), while it is not the case in the LES. As shown in Couvreux et al. (2010, Figs. 8 and 9), small-scale turbulence in the environment and inside plumes, as well as dry tongues (Couvreux et al. 2007), strongly contribute to the total vertical fluxes, particularly for moisture. Yet, those contributions are not taken into account in our parametrizations. This means that, somehow, the mixing rates have to be different from those given by LES in order to compensate for the lack in the representation of other physical processes, yet better simulate the mean profiles. Of course, a better way to deal with this would be to develop a parametrization for the dry tongues as well as for the contribution of small-scale turbulence to the vertical transport in the

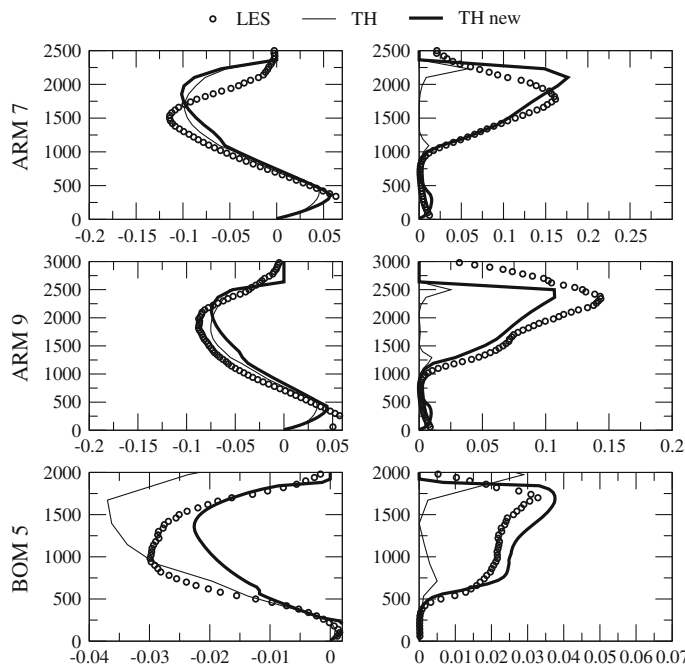


Fig. 5 Vertical profiles of the top-hat contribution to total flux (in K m s^{-1} , left) and variance (in K^2 , right) of θ_t at 1330 local time (ARM7) and 1530 local time (ARM9) for the ARM case and at the fifth hour of simulation BOMEX (BOM5): comparison of LES results using the conditional sampling (black dots) with results obtained with the original (TH, light black line) and the new (THnew, dark black line) versions of the thermal plume model

whole boundary layer. This indeed could be achieved by adapting the conditional sampling used here to those physical processes.

5 Conclusion

We proposed continuous formulations of fractional entrainment and detrainment rates from the surface to cloud top for use in mass-flux schemes of boundary-layer thermals. Such formulations are evaluated based on the conditional sampling of thermals proposed in Couvreux et al. (2010, Part I), and tested in single-column simulations using the thermal plume model of Rio and Hourdin (2008).

A relationship between ε and the divergence of the vertical velocity inside plumes is shown applying the conditional sampling to two large-eddy simulations of marine and continental shallow clouds. Results suggest that entrainment is not far from the constant fractional cover hypothesis (without detrainment), with a proportionality factor close to 1. When implementing this in the thermal plume model, the formulation improves the representation of entrainment, in particular its vertical and temporal variations, and appears to be adapted to both oceanic and terrestrial conditions.

Concerning detrainment, the conditional sampling allows us to put forward relationships between δ and both B/w_u^2 and $(\Delta r_t/r_t)/w_u^2$, suggesting that mechanisms dominating entrainment and detrainment are different. The relative contribution of these two terms cannot be

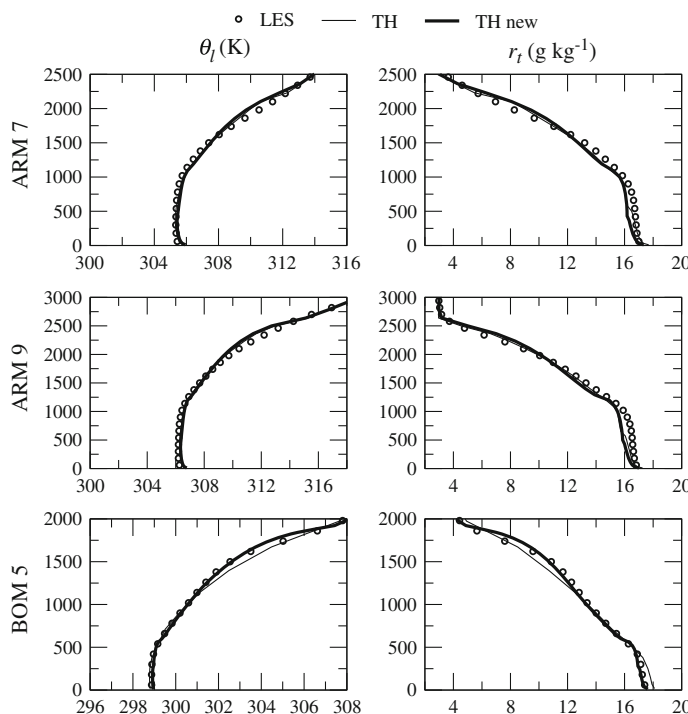


Fig. 6 Vertical profiles of liquid potential temperature (θ_l in K, left) and total water mixing ratio (r_t in g kg^{-1} , right) at 1330 local time (ARM7) and 1530 local time (ARM9) for the ARM case and at the fifth hour of simulation BOMEX (BOM5): comparison of mean LES fields (black dots) with results obtained with the original (TH, light black line) and the new (THnew, dark black line) versions of the thermal plume model

rigorously assessed at this stage. Nevertheless, the considerations converge towards the buoyancy sorting view, and further investigations are foreseen, such as considering the buoyancy of parcels after mixing with environmental air for detrainment computations. A dependency of free parameters on the fractional cover of the plume would also make sense in that context. So the determination of detrainment certainly deserves further investigation. However, the proposed formulation (Eq. 15) reproduces quite satisfactorily the relationship between detrainment and the thermal properties in the LES, and lead to results consistent with LES when tested in full single-column simulations with the thermal plume model.

For the vertical momentum equation, results clearly show the importance of taking into account the effect of turbulence and pressure on vertical velocity. However, the assumptions made cannot be verified in LES in the present study, which can be an issue since entrainment and detrainment depend on vertical velocity. This point deserves further investigation.

By improving the representation of the vertical transport effected by thermals, our study also highlights the lack of an adequate representation of other processes contributing to total vertical fluxes, such as small-scale turbulence and dry tongues. Here, the conditional sampling presented in Couvreux et al. (2010) is used to study thermals continuously from the surface to cloud top, in particular in the transition zone between the sub-cloud and the cloud layer. The same methodology could be used to identify other structures within the convective boundary layer and further improve parametrizations of boundary-layer structures and clouds.

References

- Blyth AM, Cooper WA, Jensen JB (1988) A study of the source of entrained air in Montana cumuli. *J Atmos Sci* 45:3944–3964
- Bretherton C, Smolarkiewicz P (1989) Gravity waves, compensating subsidence and detrainment around cumulus clouds. *J Atmos Sci* 46:740–759
- Bretherton C, McCaa J, Grenier H (2004) A new parameterization for shallow cumulus convection and its application to marine subtropical cloud-topped boundary layers. Part I: description and 1D results. *Mon Weather Rev* 132:864–882
- Brown A, Cederwall R, Chlond A, Duynkerke P, Golaz J-C, Khairoutdinov M, Lewellen D, Lock A, Macvean M, Moeng C-H, Neggers R, Siebesma A, Stevens B (2002) Large-eddy simulation of the diurnal cycle of shallow cumulus convection over land. *Q J Roy Meteorol Soc* 128:1075–1093
- Chatfield RB, Brost RA (1987) A two-stream model of the vertical transport of trace species in the convective boundary layer. *J Geophys Res* 92:13263–13276
- Coindreau O, Hourdin F, Haefelin M, Mathieu A, Rio C (2007) Assessment of physical parameterizations using a global climate model with stretchable grid and nudging. *Mon Weather Rev* 135:1474–1489
- Couveaux F, Guichard F, Redelsperger J-L, Flamant C, Masson V, Kiemle C, Lafore J-P (2005) Water vapour variability within a convective boundary layer assessed by large eddy simulations and IHOP observations. *Q J Roy Meteorol Soc* 131:2665–2693
- Couveaux F, Guichard F, Masson V, Redelsperger J-L (2007) Negative water vapour skewness and dry tongues in the convective boundary layer: observations and large-eddy simulation budget analysis. *Boundary-Layer Meteorol* 123:269–294
- Couveaux F, Hourdin F, Rio C (2010) Resolved versus parameterized boundary layer thermals. Part I: a parameterization oriented conditional sampling in large Eddy simulations. *Boundary-Layer Meteorol* 134:441–458
- de Rooy WC, Siebesma AP (2008) A simple parameterization for detrainment in shallow cumulus. *Mon Weather Rev* 136:560–576
- Deardorff JW (1972) Theoretical expression for the countergradient vertical heat flux. *J Geophys Res* 77:5900–5904
- Gregory D (2001) Estimation of entrainment rate in simple models of convective clouds. *Q J Roy Meteorol Soc* 127:53–72
- Grossman RL (1984) Bivariate conditional sampling of moisture flux over a tropical ocean. *J Atmos Sci* 41:3238–3253
- Heus T, Jonker HJJ (2008) Subsiding shells around cumulus clouds. *J Atmos Sci* 65:1003–1018
- Heus T, Van Dijk G, Jonker HJJ, Van den Akker HEA (2008) Mixing in shallow cumulus clouds studied by lagrangian particle tracking. *J Atmos Sci* 65:2581–2597
- Hourdin F, Couveaux F, Menut L (2002) Parameterisation of the dry convective boundary layer based on a mass flux representation of thermals. *J Atmos Sci* 59:1105–1123
- Hourdin F, Musat I, Bony S, Braconnot P, Codron F, Dufresne J-L, Fairhead L, Filiberti M-A, Friedlingstein P, Grandpeix J-Y, Krinner G, LeVan P, Li Z-X, Lott F (2006) The LMDZ4 general circulation model: climate performance and sensitivity to parametrized physics with emphasis on tropical convection. *Clim Dyn* 27:787–813
- LeMone MA, Pennell WT (1976) The relationship of trade wind cumulus distribution to subcloud layer fluxes and structure. *Mon Weather Rev* 104:524–539
- Moeng C, Wyngaard JC (1988) Spectral analysis of large-eddy simulations of the convective boundary layer. *J Atmos Sci* 45(23):3573–3587
- Neggers RAJ, Siebesma P, Jonker HJJ (2002) A multiparcel model for shallow cumulus convection. *J Atmos Sci* 59:1655–1668
- Neggers RAJ, Jonker HJJ, Siebesma AP (2003) Size statistics of cumulus clouds populations in large-eddy simulations. *J Atmos Sci* 60:1060–1074
- Nordeng TE (1994) Extended versions of the convective parametrization scheme at ECMWF and their impact on the mean and transient activity of the model in the Tropics. Technical memo. 206, ECMWF
- Paluch IR (1979) The entrainment mechanism in Colorado cumuli. *J Atmos Sci* 36:2467–2478
- Pergaud J, Masson V, Malardel S, Couveaux F (2009) A parameterization of dry thermals and shallow cumuli for mesoscale numerical weather prediction. *Boundary-Layer Meteorol* 132, 83–106
- Rio C, Hourdin F (2008) A thermal plume model for the convective boundary layer: representation of cumulus clouds. *J Atmos Sci* 65:407–425
- Siebesma AP (1998) Shallow cumulus convection. In: Plate EI, Fedorovich EE, Viegas DX, Wyngaard JC (eds) *Buoyant convection in geophysical flow*. Kluwer, Dordrecht, pp 441–486

- Siebesma A, Cuijpers J (1995) Evaluation of parametric assumptions for shallow cumulus convection. *J Atmos Sci* 52:650–666
- Siebesma AP, Jonker HJJ (2000) Anomalous scaling of cumulus cloud boundaries. *Phys Rev Lett* 85:214–217
- Siebesma A, Teixeira J (2000) An advection–diffusion scheme for the convective boundary layer, description and 1D results. In: Proceedings of 14th AMS symposium on boundary layers and turbulence, AMS
- Siebesma AP, Bretherton CS, Brown A, Chlond A, Cuxart J, Duynkerke PG, Jiang H, Khairoutdinov M, Lewellen D, Moeng C-H, Sanchez E, Stevens B, Stevens DE (2003) A large eddy simulation intercomparison study of shallow cumulus convection. *J Atmos Sci* 60:1201–1219
- Simpson J, Wiggert V (1969) Models of precipitating cumulus towers. *Mon Weather Rev* 97:471–489
- Soares P, Miranda P, Siebesma A, Teixeira J (2004) An eddy-diffusivity/mass flux parameterization for dry and shallow cumulus convection. *Q J Roy Meteorol Soc* 130:3365–3383
- Stith JL (1992) Observations of cloud-top entrainment in cumuli. *J Atmos Sci* 49:1334–1347
- Stull RB (1984) Transient turbulence theory. Part I: the concept of eddy-mixing across finite distances. *J Atmos Sci* 41:3351–3367
- Tiedtke M (1989) A comprehensive mass flux scheme for cumulus parameterization in large-scale models. *Mon Weather Rev* 117:1179–1800
- Von Salzen K, McFarlane NA (2002) Parameterization of the bulk effects of lateral and cloud-top entrainment in transient shallow cumulus clouds. *J Atmos Sci* 59:1405–1430
- Williams AG, Hacker JM (1992) The composite shape and structure of coherent eddies in the convective boundary layer. *Boundary-Layer Meteorol* 61:213–245
- Yamada T (1983) Simulations of nocturnal drainage flows by a $q^2 l$ turbulence closure model. *J Atmos Sci* 40:91–106
- Young GS (1988) Turbulence structure of the convective boundary layer. Part II: phoenix 78 aircraft observations of thermals and their environment. *J Atmos Sci* 45:727–735
- Zhao M, Austin P (2005) Life cycle of numerically simulated shallow cumulus clouds. Part I: mixing dynamics. *J Atmos Sci* 62:1291–1310